Density functional theory calculations of the activation of methanol by a Bronsted zeolitic proton

Document status and date:
Published: 01/01/1995

Document Version:
Publisher's PDF, also known as Version of Record (includes final page, issue and volume numbers)

Please check the document version of this publication:

• A submitted manuscript is the version of the article upon submission and before peer-review. There can be important differences between the submitted version and the official published version of record. People interested in the research are advised to contact the author for the final version of the publication, or visit the DOI to the publisher's website.
• The final author version and the galley proof are versions of the publication after peer review.
• The final published version features the final layout of the paper including the volume, issue and page numbers.

[Link to publication](#)

Density Functional Theory Calculations of the Activation of Methanol by a Brønsted Zeolitic Proton

S. R. Blaszkowski*,‡,§ and R. A. van Santen†

*Schuit Institute of Catalysis, Laboratory of Inorganic Chemistry and Catalysis/Theory Group,
Eindhoven University of Technology, P.O. Box 513, 5600 MB Eindhoven, The Netherlands, and
Instituto de Química, Departamento de Físico-Química, Universidade Federal do Rio de Janeiro,
Ilha do Fundão, Cidade Universitária, CT, Bloco "A", Rio de Janeiro, RJ, 21949-900 Brazil*

Density functional theory is used to determine transition states, adsorption, and dissociative complexes of Brønsted-acid-activated methanol. The respective activation barriers and adsorption and desorption energies for the reactions of hydrogen exchange and dehydration of methanol are presented. The activation barriers were found to be 11 and 212 kJ/mol for hydrogen exchange and dehydration, respectively. The methoxonium ion intermediate of the hydrogen exchange reaction was found to be a transition state corresponding to a maximum in the potential energy surface, rather than a chemisorbed species. The dehydration reaction forms a methoxy group that is a methyl group surface-bonded to the basic oxygen lattice. An analysis of the equilibrium constants shows that for both reactions methanol will adsorb initially with the hydroxyl group directed to the basic oxygen of the zeolite cluster model, perpendicular to the zeolitic surface (end-on). The dehydration reaction proceeds via a fast equilibration between this first mode of adsorption (end-on) and an adsorption mode where now the methyl group is directed to the basic oxygen of the zeolite cluster, parallel to the zeolite surface (side-on). From the calculated activation barrier and vibrational, rotational, and translational partition functions, reaction rate constants have been evaluated using transition state reaction rate theory.

1. Introduction

Methanol adsorption in zeolites has been the subject of numerous experimental[1-9] and theoretical[10-17] studies, since it is very important in the methanol-to-gasoline process (MTG).[1] In particular, the bonding and activation of methanol in protonic zeolites have been extensively investigated.

There exists a large amount of literature in this field, which is, however, often controversial. Some authors[2] have assigned their spectroscopic data to hydrogen-bonded (physically adsorbed) methanol and dimethyl ether on the zeolite surface, while some others[3,4] have suggested the formation of the methoxonium ion form, $CH_3OH_2^+$, as being more probable. The existence of methyl groups surface-bonded to the lattice oxygens is also a matter of discussion.[2,5] Bandiera and Naccache[6] have studied experimentally the kinetics of methanol dehydration catalyzed by a dealuminated H-mordenite in the 473—573 K temperature range. Their results suggested that two different sites are operative during the dehydration, probably an acidic site and its adjacent basic site on which methanol forms respectively $[CH_3 \cdot OH_2]^+$ and $[CH_3O]^-$ species, which upon condensation give dimethyl ether and water.

Here we will present a quantum chemical study of adsorption modes as well as reactivity of methanol catalyzed by an acidic zeolite cluster model. One of the first theoretical studies of this reaction has been undertaken by Vetrivel et al.[10] They used a combination of lattice simulation and ab-initio calculations to locate the low-energy adsorption inside the pores of the zeolite. They predict that two different orientations of methanol toward the surface are possible. In the first it is the methyl group which approaches the zeolitic framework, while the hydroxyl group is pointing away from it. There, the abstraction of hydrogen from the methyl group of methanol by the basic lattice oxygen takes place. In the other case, the hydroxyl group is oriented toward the surface with the zeolitic proton oriented to the methanol oxygen within a hydrogen-bonding distance. In a latter work, Gale et al.[11] showed that Vetrivel et al.[10] have used an incorrect charge balance to simulate the embedding cluster conditions, resulting in the interaction of methanol with a quadruple negatively charged lattice. This results in the incorrect abstraction of a hydrogen atom from the methyl group by the framework. Using semiempirical calculations and a much larger cluster (20 tetrahedral atoms), Gale et al.[11] found that the oxygen of the hydroxyl group of the methanol molecule is hydrogen-bonded to the framework proton, and the carbon atom acquires a significant increased positive charge, suggesting a subsequent C—O bond breaking.

The computation of the energies of the hydrogen-bonded and protonated methanol ($CH_3OH_2^+$) by a zeolite cluster model is a difficult problem from a quantum-chemical point of view. High-quality calculations are required to determine these states. The work of Sauer et al.[12] and of Haase and Sauer[13,14a] illustrates this. Using the Hartree—Fock (HF) method with a single-point second-order Møller—Plesset (MP2) correction for a three-tetrahedral (3T) atom cluster, but performing frequency calculations for a 1T atom cluster, Sauer et al.[12] initially concluded that the protonated complex, the methoxonium ion, would be formed. The proton transfer from the zeolite cluster was found to be favorable with a heat of reaction of −12 kJ/mol. In this study both the hydrogen-bonded and protonated ($CH_3OH \cdot \cdot cluster$) complexes correspond to a minimum in the potential energy surface (PES). However, this was due to the use of symmetry constraints, as discussed by Gale et al.[15] In a computational study of ¹H NMR chemical shifts of ammonia, methanol, and

---

water (using HF/single-point MP2 and a 5T atom cluster), Haase and Sauer[13] have concluded that the methoxonium ion corresponds to a saddle point in the PES and the hydrogen-bonded complex is the ground state structure. On the other hand, they have observed that the NMR shifts are in between the calculated shifts for the neutral (hydrogen-bonded) and ion-pair (protonated methanol) structures leading to the conclusion that there is equilibrium between these structures. Very recently, in an extension of the later work, Haase and Sauer[14a] have obtained structures optimized at the MP2 level. Now the ^{1}H NMR shifts for the neutral adsorption complex (hydrogen bonded) are very close to the experimental ones, whereas the ones corresponding to the ionic complex are far off.

Gale et al.[15] have used density functional theory (DFT) calculations to study the interaction of methanol with a cluster model zeolite. In their work they find that hydrogen-bonded methanol is the most stable structure and suggest that the methoxonium ion must almost certainly be a transition state. Additionally, they performed a 6-31G**/HF calculation for a 1T atom cluster. There, the protonated methanol corresponds to a transition state, lying 150 kJ/mol higher in energy than the hydrogen-bonded structure. More recently, Bates and Dwyer[16] have performed HF calculations including single-point MP2 corrections, and their conclusions agree with the older work of Sauer et al.,[12] except that in their case the proton transfer was found to be unfavorable (+6 kJ/mol).[17]

When methanol is in contact with the acidic site of the zeolite, hydrogen−deuterium, reaction 1a, or hydrogen−hydrogen exchange, reaction 1b, as well as dehydration, reaction 2, can occur (‡ indicates transition state):

$$CD_3OD + ZOH \rightarrow (CD_3ODH^+ \cdots ZO^-)^{\ddagger} \rightarrow$$
$$ZOD + CD_3OH \quad (1a)$$

$$CH_3OH + ZOH \rightarrow (CH_3OH_2^+ \cdots ZO^-)^{\ddagger} \rightarrow$$
$$ZOH + CH_3OH \quad (1b)$$

$$CH_3OH + ZOH \rightarrow (CH_3^+ \cdots OH_2^+ \cdots ZO^-)^{\ddagger} \rightarrow$$
$$ZOCH_3 + H_2O \quad (2)$$
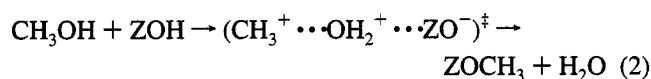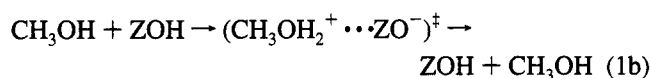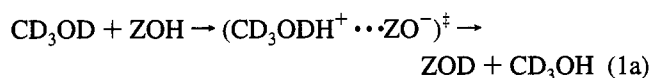
In reaction 1a the exchange between the zeolitic proton and the deuterium, hydrogen for reaction 1b, is considered. Reaction 2 represents the dehydration of methanol by the zeolite with formation of a methyl group surface bonded to the basic lattice oxygen. In the work presented here we used DFT calculations to investigate the reaction of hydrogen exchange (reaction 1b), where results for the hydrogen-bonded ground state and corresponding transition state are presented. A comparison with earlier calculations[10−17] will also be presented. For the dehydration reaction (2) the modes of adsorption as well as the transition state, adsorption, and dissociative complexes are discussed. For the adsorbed methanol, a discussion of the harmonic vibrational frequencies and equilibrium constants is presented. Additionally, from the calculated activation barriers of the transition states and the vibrational, rotational, and translational partition functions of adsorption complexes and transition states, an analysis of the reaction rate constants is given.

2. Method

2.1. Computational Details. All calculations in this work are based on density functional theory (DFT),[18] using the DGauss program (version 2.1), part of the UniChem package from Cray Research, Inc.[19] The calculations were carried out

at two different levels. The first is the local density approximation using the exchange-correlation potential in the form parametrized by Vosko, Wilk, and Nusair.[20] To the final optimized structure, nonlocal correlation and exchange corrections due to Perdew[21] and Becke,[22] respectively (NL), are included in the final total LDA energy. At the second level, the NL correction is included in a self-consistent manner (NLSCF). The LDA without any nonlocal correction showed to be inadequate for the calculation of accurate binding energies for reactions which involve hydrogen transfer.[23,24]

Molecular orbitals are expressed as a linear combination of atomic Gaussian-type orbitals. The basis sets are of double-ζ quality and include polarization functions for all non-hydrogen atoms (DZPV).[25] They were optimized for use in density functional calculation in order to minimize the basis set superposition error (BSSE),[26] as has been demonstrated by Radzio et al.[26b] in studies of the Cr_2 molecule. A second set of basis functions, the auxiliary basis set,[27] is used to expand the electron density in a set of single-particle Gaussian-type functions.

Total LDA energy gradients are computed analytically.[28] Geometry optimization calculations are carried out to a minimum in the case of reactants, adsorption and dissociative complexes, and products, and to a saddle point in the case of transition states (TS). For a TS, the norm of the gradient is minimized and not the energy.[29] The frequencies are obtained by evaluating the matrix of the second derivatives by a finite difference scheme using the analytic first derivatives.[30] Unscaled frequencies have been used and zero-point energy (ZPE) corrections included.

The molecular system used consisted of one methanol molecule and two different size tritetrahedral clusters, $H_3SiOHAl(OH)_2OSiH_3$ and $H_3SiOHAlH_2OSiH_3$, that represent the acidic zeolite. For easier reference, those clusters will be named AlOH and AlH, respectively. In the cluster AlOH, the aluminum atom was terminated by two hydroxyl groups, and in the AlH cluster by two hydrogen atoms. The peripheral bonds of the silicon atoms were saturated with hydrogens. No constraint of symmetry has been used in the final optimization of the structures studied.

2.2. Reaction Rate Constants. The reaction rate constants have been calculated using the transition state reaction rate theory (TST).[31] It is based on the application of statistical mechanics to reactants and activated complexes. The fraction of occupied acidic sites or surface coverage (θ) is related to the adsorption equilibrium constant (K_{eq}) and pressure (p) of the system according to Langmuir's equation

$$\theta/(1 - \theta) = K_{eq}p \quad (3)$$

The adsorption equilibrium constant (K_{eq}) between reactants (methanol in the gas phase, CH_3OH, and the zeolite cluster, HOZ) and the adsorbed complex ($CH_3OH−HOZ$) is given by

$$K_{eq} = (N_A V)\frac{q_{v(CH_3OH−HOZ)_{ads}}}{q_v q_r q_{t(CH_3OH)} q_{v(HOZ)}}e^{-E_{ads}/k_B T} \quad (4)$$

where N_A and k_B are Avogadro and Boltzman's constants, V is the volume, and T is the temperature of the system. E_{ads} is the adsorption energy which includes already the zero-point energy correction. In the equation, q_v, q_r, and q_t are the vibrational, rotational, and translational partition functions. For the methanol molecule all three must be evaluated. For the adsorption complex $(CH_3OH−HOZ)_{ads}$ and the cluster (HOZ), assuming

that the zeolite does not rotate or translate, only the vibrational partition function needs to be calculated.

For the cases where more than one mode of adsorption is observed, the equilibrium constant (K_{eq}(ads′:ads″)) between those modes is expressed in terms of

$$K_{eq}(\text{ads}':\text{ads}'') = \frac{q_{v(\text{CH}_3\text{OH}-\text{HOZ})_{\text{ads}''}}}{q_{v(\text{CH}_3\text{OH}-\text{HOZ})_{\text{ads}'}}} e^{(E_{\text{ads}''}-E_{\text{ads}'})/k_B T} \quad (5)$$

where (′) refers to the first mode of adsorption and (″) to the second.

The reaction rate constant (k_r) expressed in terms of "rate per acidic proton" for methanol activation is then given by

$$k_r = \left(\frac{k_B T}{h}\right)\frac{q^{\ddagger}_{v(\text{TS})}}{q_{v(\text{CH}_3\text{OH}-\text{HOZ})_{\text{ads}}}} e^{-E_{\text{bar}}/k_B T} \quad (6)$$

where h is Planck's constant and E_{bar} is the activation barrier which already includes the ZPE corrections. Just as for K_{eq}, which assumed that the zeolite does not rotate and translate, only the vibrational partition function has to be evaluated for the transition state (TS) and adsorption complex (CH$_3$OH–HOZ)$_{\text{ads}}$.

The natural logarithm of the reaction rate constant, ln k_r, is a linear function of the reciprocal temperature ($1/T$) according to the equation

$$\ln k_r = -E_{\text{act}}/k_B T + \ln A^{\text{TST}} \quad (7)$$

where E_{act} is the Arrhenius activation energy and A^{TST} is the pre-exponential factor. The latter is related to the change in activation entropy of the system of the adsorbed ground state and transition state. If, instead of merely k_r, the product of k_r and K_{eq} (called k_{eff} in this paper) is plotted, $E^{\text{eff}}_{\text{act}}$ (effective Arrhenius activation energy) and $A^{\text{TST}}_{\text{eff}}$ (effective pre-exponential factor) are obtained. In general $E^{\text{eff}}_{\text{act}}$ and $A^{\text{TST}}_{\text{eff}}$ are complex functions of the concentrations and rate constant parameters of the elementary reactions that form the reaction sequence. Under conditions where the overall reaction rate is linear in the methanol pressure, the effective rate constant equals the product of K_{eq} and k_r. In the case of dimethyl ether formation at low pressure, the reaction is second order in methanol. Now the effective rate constant is equal to the product of $(K_{eq})^2$ and k_r.

Finally, a comparison between the effective pre-exponent obtained with the transition state theory ($A^{\text{TST}}_{\text{eff}}$) and the hard sphere pre-exponent (A^{HS}), which gives the number of collisions of a methanol molecule approximated as a hard sphere, can be made. The latter sets an upper limit for the former. The hard sphere pre-exponent is given by

$$A^{\text{HS}} = {}^1/_4 N_A \pi d^2 (8k_B T/\pi m)^{1/2} \quad (8)$$

where m is the mass of CH$_3$OH and d is the kinetic diameter of the methanol molecule in the gaseous phase (3.63 Å).[8] A small ratio $A^{\text{TST}}_{\text{eff}}/A^{\text{HS}}$ means a significant decrease in reaction entropy, due to loss in rotational or translational degrees of freedom.

3. Results

3.1. Hydrogen Exchange. Figure 1a,b,c shows the AlOH/NLSCF structures involved in the reaction of hydrogen exchange of methanol catalyzed by an acidic zeolite cluster model. In this reaction methanol interacts with the lattice via its hydroxyl
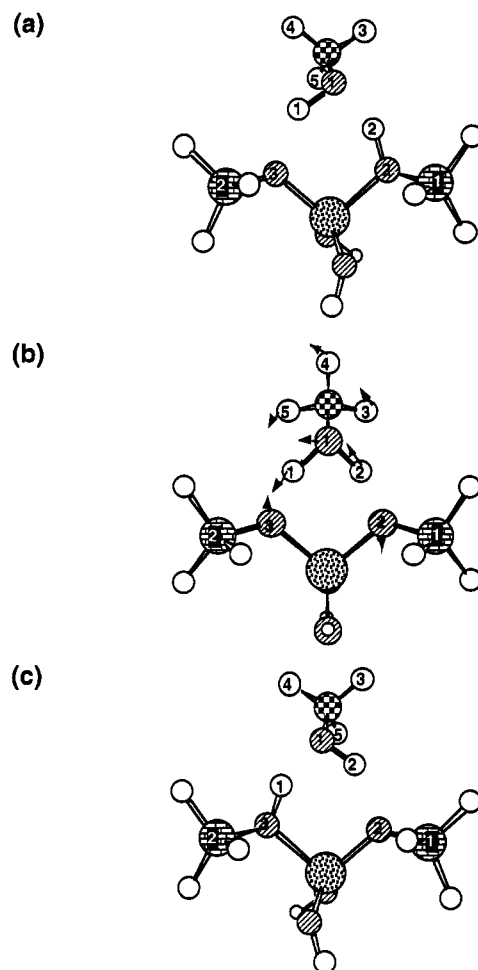
Figure 1. Hydrogen exchange: adsorption (a) and dissociative (c) complexes and TS (b).

group. Figure 1a represents the methanol molecule physically adsorbed (hydrogen-bonded) to the zeolite in an end-on position. Figure 1c shows the corresponding dissociative complex. Parts a and c of Figure 1 are mirror images of each other and, consequently, have the same properties such as energy and geometry. It is, therefore, necessary to calculate the structure and properties of only one of them. In the hydrogen exchange reaction reactants and products are exactly the same, and only if one of the reactants is deuterated can the products be experimentally observed. Figure 1b shows the calculated transition state, rather than a chemisorbed complex, for the hydrogen exchange reaction. The arrows in Figure 1b represent the movement of the atoms according to the reaction coordinate (obtained from the imaginary frequency). It represents the transfer of the zeolitic proton to methanol and the symmetrical return of the hydrogen atom from methanol to the zeolite. Both oxygens of the lattice are involved: one as a proton acceptor (basic) and the other as a proton donor (acid). In order to more easily locate the transition state for this reaction, a "pseudo" C_s symmetry was imposed, where the atoms Al, OH's, O1, C, and H4 were frozen in the same plane. All other variables were freely optimized. As soon as the transition state has been obtained, the system was allowed to relax, but almost no change in the geometry (and gradient) was found. The final transition state clearly has C_s symmetry within a small error tolerance.

Table 1 shows the total energies and ZPE obtained for all fragments involved in both reactions, hydrogen exchange and dehydration. In Table 2, the energetic and dynamic information obtained for the TSs and adsorption and dissociative complexes is presented. Figure 2 shows the ZPE corrected reaction energy

Brønsted-Acid-Activated Methanol

J. Phys. Chem., Vol. 99, No. 30, 1995 **11731**

TABLE 1: Total Energies (En, hartrees) and ZPE (kJ/mol) of the Fragments

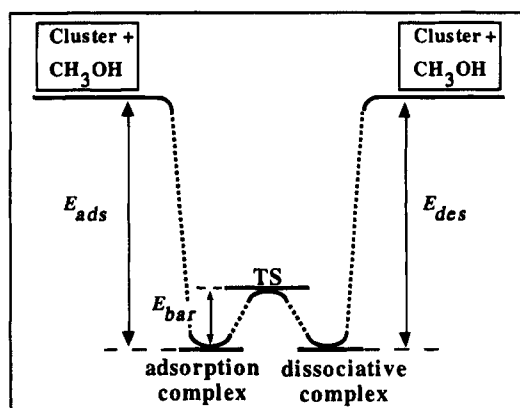|	En		ZPE	
	NL	NLSCF	NL	NLSCF
cluster AlH	−977.424 512	−977.436 479	216.60	218.92
cluster AlOH	−1128.047 190	−1128.058 981	252.97	254.37
surface methoxide AlH	−1016.732 150	−1016.743 888	292.88	294.26
surface methoxide AlOH	−1167.355 312	−1167.368 849	328.11	329.32
CH_3OH	−115.749 107	−115.752 272	131.18	131.31
H_2O	−76.442 443	−76.443 617	54.64	54.43

TABLE 2: Total Energies (En, hartrees) and ZPE (kJ/mol) for the Calculated Adsorption (ADS) and Dissociative (DIS) Complexes, and Transition States (TS) for the Reactions of Hydrogen Exchange and Dehydration (for the TS, Also the Imaginary Frequencies (IF, cm⁻¹) Are Presented)

		AlH		AlOH	
		NL	NLSCF	NL	NLSCF
			Hydrogen Exchange		
ADS end-on	En	−1093.203 635	−1093.219 422	−1243.825 066	−1243.842 154
	ZPE	348.80	356.24	388.65	393.63
TS	En	−1093.202 405	−1093.214 480	−1243.818 699	−1243.833 380
	ZPE	346.64	346.77	382.12	381.45
	IF	−84	−400	−90	−356
			Dehydration		
TS′	En	−1093.192 880		−1243.813 282	
	ZPE	355.39		390.83	
	IF	−36		−86	
ADS side-on	En	−1093.193 929	−1093.208 870	−1243.816 332	−1243.831 780
	ZPE	354.51	358.05	392.63	393.88
TS″	En	−1093.122 822	−1093.136 987	−1243.744 398	−1243.760 774
	ZPE	353.13	355.14	390.58	391.50
	IF	−544	−489	−524	−483
DIS	En	−1093.181 455	−1093.198 840	−1243.804 866	−1243.823 903
	ZPE	352.84	356.60	390.12	392.04

	AlH		AlOH	
	NL	NLSCF	NL	NLSCF
E_{ads}[a]	-77.76	-74.54	-71.01	-73.22
E_{bar}	+1.05	+3.47	+10.19	+10.86
E_{act}	+1.89	+3.64	+12.39	+12.70
A_{eff}^{TST}	$1.05 \cdot 10^{+02}$	$6.08 \cdot 10^{+02}$	$2.62 \cdot 10^{+02}$	$4.04 \cdot 10^{+02}$

a - $E_{ads} = E_{des}$

Figure 2. Adsorption energy (E_{ads}), electronic activation barrier including ZPE corrections (E_{bar}), Arrhenius activation energy (E_{act}) (in kJ/mol), and effective Arrhenius pre-exponent (A_{eff}^{TST}, in m³ mol⁻¹ s⁻¹) for the reaction of hydrogen exchange.

diagram corresponding to the hydrogen exchange reaction. The adsorption energy (E_{ads}) corrected for ZPE is on the order of −73 kJ/mol for the structures where the NLSCF correction is used independent of the cluster size. The experimental adsorption energy of methanol in H-ZSM5 zeolite obtained by Messow et al.[7] is −63 kJ/mol and by R. J. Gorte (referenced in 14b) is on the order of −115 kJ/mol. The adsorption energies obtained in earlier HF calculations for the same cluster model for the zeolite[10,12,16] are in the range −35 to −61 kJ/mol, and for a smaller zeolite cluster model,[17] −72 kJ/mol. The other DFT calculation[15] finds −63.5 kJ/mol. The result obtained in the present study is 10 kJ/mol lower than the experimental value of Messow et al.[7] and previous HF results using the same cluster,[10,12] and it is very close to the result obtained using a smaller cluster.[17] The adsorption energy obtained by Gorte[14b] is considerably lower than the other experiment[7] and all theoretical studies referenced in the present study.[10,12,15−17] It is possible that in the samples used methanol interacts strongly

with Lewis acidic sites. The difference between the results presented here and those obtained by Gale et al.,[15] both DFT/DZPV/NLSCF using a 3T atom cluster, is probably due to different convergence criteria.

The activation barriers including ZPE corrections (E_{bar}) are more sensitive to cluster size than to the kind of correction included. As can be seen in Figure 2, the E_{bar} for AlH/NL and NLSCF is 1 and 3 kJ/mol, respectively. It increases to 10 and 11 kJ/mol if the AlOH cluster is considered. This is a rather small barrier. Even considering the tendency of DFT to underestimate the barriers,[32] the real value probably wouldn't be much higher. Gale et al.,[15] for a 1T atom cluster and HF/6-31G**, found a transition state which lies 150 kJ/mol higher in energy than the hydrogen-bonded complex. Bates and Dwyer[16] have attributed the presence of imaginary frequencies to imposition of symmetry. Nevertheless, their E_{bar} for the protonated complex is a barrier of 5.7 kJ/mol rather than a

TABLE 3: Geometries for the Adsorption Complex (End-On) and Transition State for the Reaction of Hydrogen Exchange (Distances in Angstroms and Angles in Degrees)

| | adsorption complex end-on | | | | | | transition state | | | | |
| | AlH | | AlOH | | | | AlH | | AlOH | | |
	NL	NLSCF	NL	NLSCF	ref 15	ref 16	NL	NLSCF	NL	NLSCF	ref 16
O1−H1	1.076	1.004	1.045	1.005	1.005	0.953	1.135	1.122	1.129	1.123	1.027
O1−H2	1.215	1.527	1.297	1.527	1.491	1.719	1.135	1.127	1.129	1.123	1.027
H2−O2	1.215	1.050	1.146	1.052	1.061	0.971	1.306	1.348	1.316	1.351	1.475
H1−O3	1.424	1.786	1.522	1.786	1.818	2.048	1.308	1.356	1.314	1.352	1.475
O1−C	1.428	1.449	1.427	1.449	1.455	1.405	1.432	1.464	1.435	1.464	1.435
C−H3	1.108	1.102	1.104	1.100			1.106	1.102	1.105	1.101	
C−H4	1.104	1.105	1.106	1.104			1.104	1.100	1.105	1.101	
C−H5	1.105	1.105	1.108	1.105			1.106	1.101	1.105	1.101	
Si1−O2	1.682	1.727	1.696	1.726		1.679	1.676	1.691	1.674	1.690	
Al−O2	1.878	1.980	1.858	1.926		1.946	1.858	1.889	1.832	1.863	
Al−O3	1.839	1.817	1.788	1.788		1.749	1.860	1.890	1.834	1.864	
Si2−O3	1.669	1.673	1.665	1.672		1.624	1.677	1.690	1.674	1.690	
Si1−O2−Al	123.01	124.57	121.41	123.03		128.86	123.39	124.17	123.28	125.05	
O2−Al−O3	95.00	95.92	96.72	97.19		98.20	95.03	95.02	94.86	94.98	
Si2−O3−Al	125.95	125.85	124.21	125.61		139.69	124.10	125.43	123.49	124.82	

TABLE 4: Mulliken Charges for the Adsorption Complex (End-On) and Transition State for the Reaction of Hydrogen Exchange

| | adsorption complex end-on | | | | transition state | | | |
| | AlH | | AlOH | | AlH | | AlOH | |
	NL	NLSCF	NL	NLSCF	NL	NLSCF	NL	NLSCF
O1	−0.558	−0.624	−0.575	−0.621	−0.561	−0.586	−0.560	−0.590
H1	0.483	0.484	0.489	0.487	0.489	0.498	0.491	0.504
H2	0.495	0.515	0.503	0.519	0.489	0.502	0.491	0.504
C	−0.563	−0.458	−0.562	−0.465	−0.540	−0.449	−0.537	−0.445
H3	0.258	0.223	0.253	0.224	0.246	0.229	0.250	0.232
H4	0.260	0.222	0.256	0.222	0.261	0.240	0.258	0.237
H5	0.252	0.220	0.255	0.226	0.247	0.230	0.251	0.232
Si1	0.281	0.409	0.303	0.434	0.279	0.407	0.285	0.411
O2	−0.733	−0.774	−0.713	−0.769	−0.737	−0.808	−0.718	−0.794
Al	0.286	0.437	0.724	0.897	0.304	0.454	0.756	0.935
O3	−0.727	−0.754	−0.693	−0.736	−0.738	−0.807	−0.719	−0.795
Si2	0.281	0.394	0.287	0.404	0.279	0.407	0.285	0.409

minimum. The E_{bar} obtained by Senchenya et al.[17] is 10.2 kJ/mol (1T atom cluster).

Brand et al.[33] showed that the inclusion of a shell of oxygens increases the proton affinity, whereas the inclusion of a new silicon shell decreases it. The conclusion is that the AlH cluster, where Al is terminated by hydrides (H) rather than hydroxyls (OH), possibly gives a better description of the zeolitic OH acidity. From this it should be expected that the AlH/NLSCF gives E_{bar} closer to the true value than AlOH/NLSCF. The true value of E_{bar} should be located in between 3.5 and 10.9 kJ/mol. It is important to notice that for the overall exchange reaction the limiting step will not be the activation barrier, E_{bar}, but the desorption rate, with an activation energy on the order of 70 kJ/mol.

Distances and angles between the most important atoms are shown in Table 3. For the adsorption complex, the distances O1,2,3−H1,2 are strongly affected by the kind of correction included, as it has been already referenced previously.[15] This is due to the presence of O•••H nonbonding interactions. The distances O1−H2 and H2−O2 in the adsorption complex, calculated at the AlH/NL level, have the same value, 1.215 Å, meaning that H2 is found exactly halfway in between O1 and O2. If the NLSCF correction is included, these distances change to 1.527 Å (O1−H2) and 1.050 Å (H2−O2), characterizing the protonated cluster and methanol molecule. At the AlH/NL level, the distances O1−H1 and H1−O3 are 1.076 and 1.424 Å, respectively. These resemble the methanol molecule more. If the NLSCF correction is included, these distances change to 1.004 Å (O1−H1) and 1.786 Å (H1−O3). An analogous behavior is found for AlOH/NL and NLSCF, as can be seen in

Table 3. The distance O1−C is around 0.02 Å longer for the cases where NLSCF is included than for NL. Also in the cluster, the distances Al−O and Si−O are slightly larger for the NLSCF correction. A small difference was found comparing the results obtained in this study with those of Gale et al.[15] for AlOH/NLSCF. The principal difference was found for the distances O1−H2 and H2−O2, which are in between the NL and NLSCF results obtained in this study. The difference between these distances becomes larger if comparisons are made with the results obtained using the HF method,[16] as can be seen in Table 3.

The geometry obtained for the transition state for the hydrogen exchange reaction is also shown in Table 3. The distances O1−H1,2 are almost the same, on the order of 1.13 Å. The distances H2−O2 and H1−O3 are also very similar, on the order of 1.35 Å. The type of correction included seems to affect the last group of distances a little more than the previous group. The HF[16] O1−H1,2 distances are around 0.1 Å shorter and H1,2−O3,2 distances are around 0.1 Å larger than the DFT distances. The same behavior of DFT compared to HF has been observed previously in a study of methane hydrogen exchange.[24] As can be seen from Table 3, although no symmetry constrains have been used, the transition state clearly has C_s symmetry.

Table 4 gives the computed Mulliken charges. It is important to keep in mind the arbitrariness of the Mulliken charge analysis and use those numbers only on an illustrative basis. Differences in calculated charges are, possibly, more reliable than the absolute values. The behavior is similar for both clusters, except for the Al atom, which is much more positively charged in the

Brønsted-Acid-Activated Methanol

J. Phys. Chem., Vol. 99, No. 30, 1995 **11733**

TABLE 5: Equilibrium Constants between Reactants and the End-On Adsorption Mode (K_{eq}, in m^3 mol^{-1}) and Rate Constants (k_r, s^{-1}) for Different Temperatures (T, in K) for the Reaction of Hydrogen Exchange

| | K_{eq} | | | | k_r | | | |
| | AlH | | AlOH | | AlH | | AlOH | |
T	NL	NLSCF	NL	NLSCF	NL	NLSCF	NL	NLSCF
273	$1.26 \times 10^{+4}$	$1.08 \times 10^{+4}$	$3.73 \times 10^{+3}$	$1.07 \times 10^{+3}$	$1.16 \times 10^{+12}$	$3.75 \times 10^{+11}$	$6.45 \times 10^{+9}$	$5.25 \times 10^{+10}$
473	6.28×10^{-3}	1.38×10^{-2}	6.20×10^{-3}	1.31×10^{-3}	$1.64 \times 10^{+12}$	$7.18 \times 10^{+11}$	$6.12 \times 10^{+10}$	$5.40 \times 10^{+11}$
673	2.15×10^{-5}	7.22×10^{-5}	3.39×10^{-5}	6.64×10^{-6}	$1.90 \times 10^{+12}$	$9.31 \times 10^{+11}$	$1.57 \times 10^{+11}$	$1.42 \times 10^{+12}$
873	1.18×10^{-6}	4.93×10^{-6}	2.36×10^{-6}	4.45×10^{-7}	$2.06 \times 10^{+12}$	$1.09 \times 10^{+12}$	$2.66 \times 10^{+11}$	$2.44 \times 10^{+12}$
1073	2.16×10^{-7}	1.03×10^{-6}	5.00×10^{-7}	9.17×10^{-8}	$2.18 \times 10^{+12}$	$1.22 \times 10^{+12}$	$3.74 \times 10^{+11}$	$3.50 \times 10^{+12}$
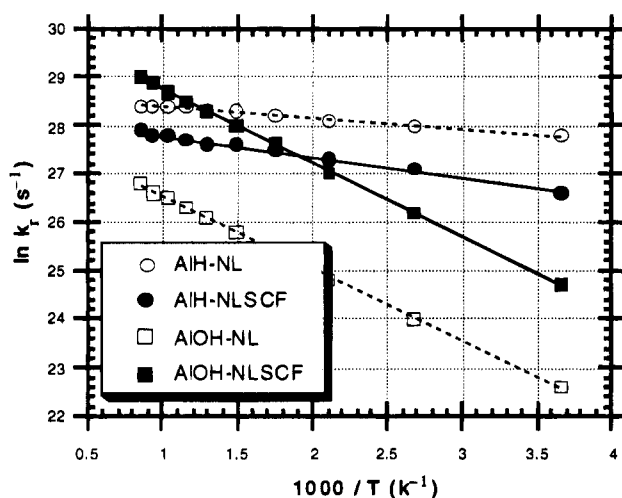
Figure 3. Arrhenius plot: temperature (T) dependence of the natural logarithm of the rate constant, ln k_r, for the reaction of hydrogen exchange. The symbols (O, ●, □, ■) represent the calculated ln k_r; the lines (—, - - -), the linear fit.

AlOH cluster than in AlH. This is possibly due to the presence of the oxygen atom in the OH terminal groups in the AlOH cluster that is more electronegative than the hydrogen atom in the terminal hydrides in the AlH cluster. In spite of this difference in charge, no significant differences in geometry were found, as discussed. In the adsorption complex, calculated at the NL level, the charges for the atoms H1 and H2 are nearly the same. When the NLSCF correction is applied, the difference is slightly larger. Analogous behavior is found for the O1 and C atoms. For the transition state, the charges for H1 and H2 are basically the same as a reflection of the geometry. The charges also reflect the C_s symmetry of this species.

Table 5 shows the calculated equilibrium constants (K_{eq}) between reactants ($CH_3OH + HOZ$) and the adsorption complex ($CH_3OH-HOZ)_{ads}$ as well as the rate constants (k_r) between the adsorption complex and transition state obtained for different temperatures for the reaction of hydrogen exchange. As can be seen from Table 5, the rate constants obtained are very large and are, in general, larger for the AlOH cluster than for AlH. The equilibrium constants, on the other hand, are relatively small.

The Arrhenius plot (ln k_r versus $1000/T$) is shown in Figure 3. From a linear fit of the curves, the Arrhenius activation energy (E_{act}) can be obtained. The difference in slope of the AlOH and AlH curves is due to different activation barriers. A separated plot and linear fit of the k_{eff} gives the effective pre-exponents (A_{eff}^{TST}). These values can be found in Figure 2. The activation barrier (E_{bar}) and Arrhenius activation energy differ by a few kilojoules per mole. The effective pre-exponent ratios (A_{eff}^{TST}/A^{HS}) for various temperatures for both reactions, hydrogen exchange and dehydration, are shown in Table 6. For the hydrogen exchange reaction, the ratios obtained ($10^{-5}-10^{-6}$) are very small, showing a considerable decrease in entropy of

the system due to loss of rotational and translational degrees of freedom. This indicates that the obtained transition state is tight and that in the TS the methanol molecule is rigidly attached to the zeolite cluster.

3.2. Dehydration. In principle, methanol can adsorb on the zeolite cluster in two different modes, end-on shown in Figure 4a (already discussed in section 3.1) as well as side-on, shown in Figure 4c. In this latter case it is the CH group that is directed to the basic oxygen of the zeolite cluster and the oxygen atom of the methanol hydroxyl group points in the direction of the zeolitic proton. From the computed adsorption energies (E_{ads}' and E_{ads}'', Figure 5) and equilibrium constants between reactants and each one of the adsorption modes (K_{eq}, Tables 5 and 7) one concludes that the equilibrium constants for the side-on mode are very small compared to the end-on. For the side-on/end-on equilibrium, an activation barrier of only 6 kJ/mol is obtained for the AlOH cluster at the NL level. The equilibrium constants between both modes of adsorption (side-on/end-on) are shown in Table 8. From the table one concludes that at 273 K, for example, for each 10^6 molecules adsorbed only one will be adsorbed in the side-on way, while the rest will be adsorbed in the end-on way. This means that methanol adsorbs in the zeolite mainly via the end-on adsorption mode, and then, for the case of the dehydration reaction, it proceeds through the side-on mode of adsorption.

The first transition state (TS') obtained for the reaction of dehydration is represented in Figure 4b. The arrows in the figure represent the reaction coordinate, which shows the rotational movement on going from the end-on adsorption mode (perpendicular to the zeolite cluster) to the side-on adsorption mode (which is parallel to the zeolitic cluster). The C–O bond makes an angle of approximately 45° with the plane O2–Al–O3. Figure 4d shows the second calculated transition state for this reaction (TS'') and corresponding reaction coordinate, which is represented in the figure by arrows. The reaction coordinate illustrates the movement of the proton (H2) toward the oxygen of the methanol, in the direction of formation of a H_2O molecule. The carbon atom tends to bind to the basic oxygen atom (O3) of the zeolite cluster, resulting in a CH_3–zeolite complex. The CH_3 group clearly has sp^2 hybridization and resembles the intermediate carbenium ion, which has already been discussed for the activation of methane.[24,34] The CH_3–zeolite··H_2O complex (or dissociative complex) can be better seen in Figure 4e. No symmetry constraint has been used in the optimization of the structures involved in this reaction.

The total energies (En) and ZPEs for the calculated transition states and adsorption and dissociative complexes are presented in Table 2. Additionally, the imaginary frequencies for the transition states are also presented in the table. In the energetic profile (corrected for ZPE) found in Figure 5 it is possible to see that the adsorption energy (E_{ads}') that corresponds to the first adsorption mode, end-on, is -73 kJ/mol. For the second mode, the side-on, E_{ads}'' is -45 kJ/mol. The energy barrier with respect to the end-on adsorption mode (E_{bar}'') is $+212$ kJ/mol (for the AlOH/NLSCF level). Small changes of the E_{ads}',

TABLE 6: Pre-exponent Ratio ($A_{\text{eff}}^{\text{TST}}/A^{\text{HS}}$) for Different Temperatures (T, in K)

	hydrogen exchange				dehydration			
	AlH		AlOH		AlH		AlOH	
T	NL	NLSCF	NL	NLSCF	NL	NLSCF	NL	NLSCF
273	3.97×10^{-6}	2.30×10^{-5}	9.89×10^{-6}	1.53×10^{-5}	3.93×10^{-6}	1.37×10^{-3}	2.77×10^{-6}	1.18×10^{-5}
473	3.01×10^{-6}	1.74×10^{-5}	7.52×10^{-6}	1.16×10^{-5}	2.99×10^{-6}	1.04×10^{-3}	2.10×10^{-6}	8.94×10^{-6}
673	2.53×10^{-6}	1.46×10^{-5}	6.30×10^{-6}	9.73×10^{-6}	2.50×10^{-6}	8.73×10^{-4}	1.76×10^{-6}	7.50×10^{-6}
873	2.22×10^{-6}	1.28×10^{-5}	5.53×10^{-6}	8.54×10^{-6}	2.20×10^{-6}	7.67×10^{-4}	1.55×10^{-6}	6.58×10^{-6}
1073	2.00×10^{-6}	1.16×10^{-5}	4.99×10^{-6}	7.70×10^{-6}	1.98×10^{-6}	6.92×10^{-4}	1.40×10^{-6}	5.94×10^{-6}
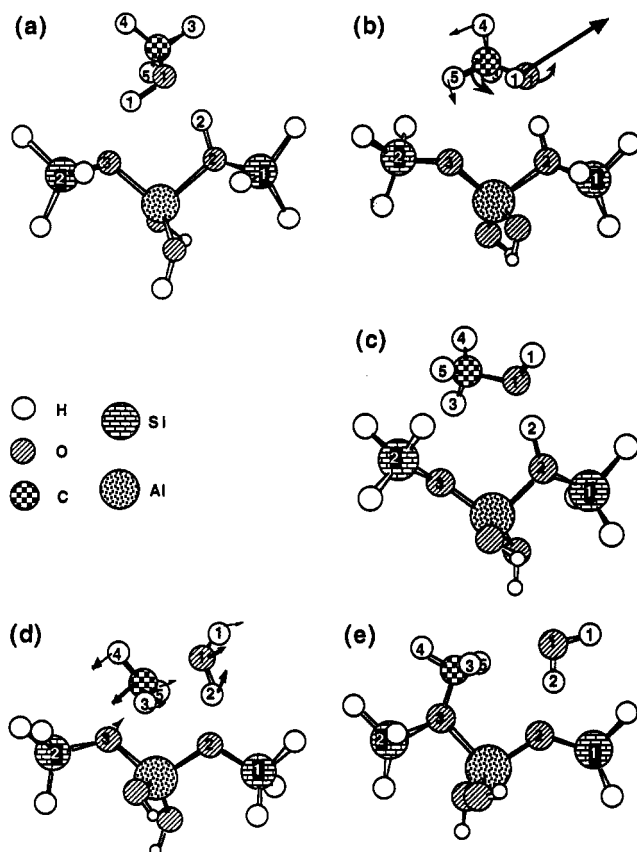
Figure 4. Dehydration: end-on (a) and side-on (c) adsorption complexes, TS′ (b), TS″ (d), and dissociative complex (e).

E_{ads}'', and E_{bar}'' according to cluster size and kind of correction can be observed in the corresponding table. The experimentally measured overall activation energy for the dehydration of methanol to dimethyl ether catalyzed by a dealuminated H-mordenite[6] is due to the reaction of two methanol molecules to give dimethyl ether and water. The experimental activation barrier, +80.3 kJ/mol, should be compared with the theoretical difference ($|E_{\text{bar}}''| - 2|E_{\text{ads}}'|$), which is +66 kJ/mol. This value is, then, nearly 14 kJ/mol lower than the experimental value.

The activation barrier with respect to the reactants (cluster + CH₃OH) obtained by Senchenya et al.[17] with their 1T atom-HF/6-31+G**/MP2 calculation is +160.9 kJ/mol, 20 kJ/mol higher than the DFT value. Their E_{ads}'' value of −54.3 kJ/mol is, conversely, almost 10 kJ/mol lower than the DFT (nearly −45 kJ/mol).

The water desorption energy, $E_{\text{des}}(\text{H}_2\text{O})$, strongly depends on the kind of correction included, NL or NLSCF. The difference is on the order of 10 kJ/mol. The final energy difference of the reaction, ΔE, depends more on cluster size (AlH or AlOH). Using AlH/NLSCF the reaction is endothermic by 1.7 kJ/mol. For the other calculated methods and clusters (AlH/NL, AlOH/NL, and AlOH/NLSCF) it is exothermic by 2.8, 5.2, and 5.2 kJ/mol, respectively (see table in Figure 5).

The geometries for the structures represented in Figure 4b−e can be found in Table 9. The end-on mode of adsorption (Figure 4a) has been discussed previously in section 3.1. The AlOH/NL transition state (TS′, Figure 4b) has a geometry that is very similar to that of the side-on adsorption complex, except for the fact that the dihedral angle C−O1−O2−O3 is nearly 45° for the TS′ compared to 90° of the adsorption mode. The AlH/NL transition state shows larger differences in geometry compared to the adsorption complex. For the side-on adsorption complex (Figure 4c), a larger difference seems to occur in the distances O1−H2 and O3−C (or O3−H3) relative to the kind of correction included. Inclusion of NLSCF correction increases the O1−H2 distance approximately 0.19 Å for the AlH cluster and 0.16 Å for the AlOH cluster. The O3−C distance for the same correction method increases by 0.27 and 0.26 Å, respectively, for the AlH and AlOH clusters. The Al−O2 distance, close to the proton, is a little larger than the Al−O3 distance. Angles are more sensitive to cluster size than to the kind of correction. In the second transition state (Figure 4d), the distance C−O1 increases by 0.45 Å, while the O3−C distance decreases by 1.28 Å if compared to the side-on adsorption complex. The distance O1−H2 decreases nearly 0.5 Å, and the water molecule is almost formed. As a consequence, the H2−O2 distance increases by almost 0.65 Å for all levels of calculation, showing almost total transference of the proton from the zeolite to the oxygen of methanol in the direction of formation of the water molecule. The O2−Al−O3 angle suffers an increase of 5−10°, and the Si2−O3−Al decreases by more than 10°, showing the tendency of the O3 atom to get closer to the carbon atom. As has been said before, the C atom of the CH₃ group has nearly sp² hybridization, with angles H−C−H varying between 116 and 126°. The Al−O distances are nearly the same.

Finally, the geometry of the dissociative complex (Figure 4e) can be analyzed. The O1−H2 distance is slightly larger than O1−H1, showing still a small interaction of the H₂O molecule with the methoxide complex. The distance C−O1 increases enormously, indicating a total separation from the water molecule. The C−O3 distance is now very short (≈1.45 Å) compared to the side-on adsorption complex and TS″, characteristic of a methyl group attached to the zeolitic oxygen lattice. The distances Al−O2,3 have suffered an inversion with respect to the adsorption complex, with Al−O3 being larger than Al−O2. This is due to the presence of the methyl group attached to O3. As a consequence, the Si2−O3−Al angle is now smaller. It is important to note that the aforementioned behavior of the Al−O and O−Si distances as well as Si−O−Al and O−Al−O angles actually represents a relaxation of the zeolitic cluster.

The Mulliken charges of some atoms are presented in Table 10. The difference in charge for the Al atom according to the cluster size has already been discussed for the hydrogen exchange reaction. On going from the TS′, to the side-on adsorption complex, to TS″, and finally to the dissociative complex, the O1 atom tends to acquire a more negative charge. This can be explained as a result of the replacement of the
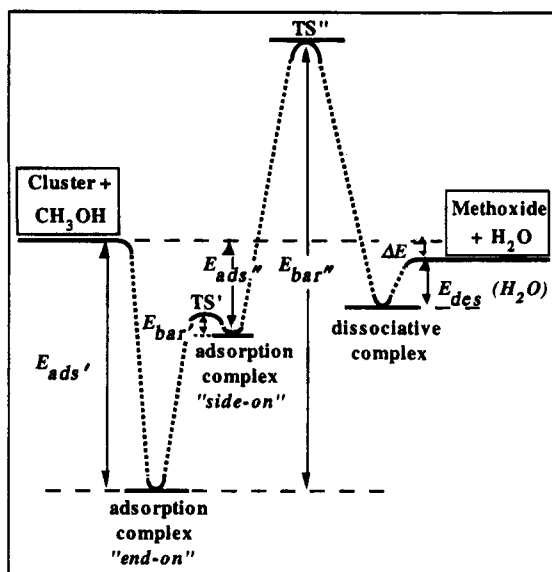
Brønsted-Acid-Activated Methanol

J. Phys. Chem., Vol. 99, No. 30, 1995 **11735**

	AlH		AlOH	
	NL	NLSCF	NL	NLSCF
E_{ads}'	-77.76	-74.54	-71.01	-73.22
E_{bar}'	+3.63	-	+6.21	-
E_{ads}''	-46.59	-45.04	-44.11	-45.74
E_{bar}''	+216.48	+215.30	+213.72	+211.53
$E_{des}(H_2O)$	-12.70	-21.85	-11.30	-21.74
ΔE	-2.81	+1.68[a]	-5.21	-5.15
E_{act}	+219.28	+218.10	+216.42	+214.75
A_{eff}^{TST}	$1.04 \cdot 10^{+02}$	$3.63 \cdot 10^{+04}$	$7.33 \cdot 10^{+01}$	$3.12 \cdot 10^{+02}$

a - The reaction in this level was found to be endothermic.

Figure 5. Adsorption (E_{ads}', E_{ads}'') and desorption ($E_{des}(H_2O)$) energies, electronic activation barriers including ZPE corrections (E_{bar}', E_{bar}''), Arrhenius activation energy with respect to the end-on adsorption complex and TS'' (E_{act}) (in kJ/mol), and effective Arrhenius pre-exponent (A_{eff}^{TST}, in m^3 mol^{-1} s^{-1}) for the reaction of dehydration.

TABLE 7: Equilibrium Constants between Reactants and the Side-On Adsorption Mode (K_{eq}, in m^3 mol^{-1}) and Rate Constants (k_r, in s^{-1}) for Different Temperatures (T, in K) for the Reaction of Dehydration

	K_{eq}				k_r			
	AlH		AlOH		AlH		AlOH	
T	NL	NLSCF	NL	NLSCF	NL	NLSCF	NL	NLSCF
273	2.48×10^2	2.53×10^2	3.78×10^3	2.34×10^2	3.73×10^{-30}	2.40×10^{-28}	1.77×10^{-30}	1.03×10^{-28}
473	5.86×10^6	9.34×10^6	1.16×10^6	6.61×10^6	1.61×10^{-12}	8.55×10^{-11}	4.48×10^{-13}	1.93×10^{-11}
673	2.61×10^7	5.06×10^7	5.29×10^8	3.20×10^7	2.61×10^5	1.26×10^3	5.98×10^6	2.25×10^4
873	5.76×10^8	1.25×10^7	1.21×10^8	7.39×10^8	2.18×10^1	1.01×10^1	4.53×10^2	1.58
1073	2.52×10^8	5.84×10^8	5.42×10^9	3.33×10^8	6.29×10^1	2.86×10^3	1.24×10^1	4.16×10^2

TABLE 8: Equilibrium Constants (K_{eq}(ads':ads'')) between End-On and Side-On Adsorption Modes for Different Temperatures (T, in K)

	AlH		AlOH	
T	NL	NLSCF	NL	NLSCF
273	1.97×10^6	2.35×10^6	1.01×10^6	2.18×10^5
473	9.34×10^4	6.75×10^4	1.78×10^4	5.03×10^3
673	1.21×10^2	7.02×10^3	1.56×10^3	4.82×10^2
873	4.89×10^2	2.53×10^2	5.14×10^3	1.66×10^1
1073	1.17×10^1	5.65×10^2	1.08×10^2	3.63×10^1

methyl group by a hydrogen atom, which is less electronegative than the carbon atom of the methyl group. The carbon partial charge, on the other hand, becomes less negative in the TS'', whereas the hydrogen atoms attached to it become more positive. As a result, the charge on the CH_3 group is more positive in the TS'' than in the adsorption and dissociative complexes. This group has characteristics of a carbenium ion, and it is strongly stabilized by both the zeolitic cluster and the OH_2 group. This would be an explanation of why the activation energy relative to reactants (+140 kJ/mol) is much lower for this reaction than it is for methane dehydrogenation (343 kJ/mol), where also a primary carbenium is formed.[24] In the dissociative complex, Si2 and O3 become less positively and negatively charged, respectively. If more attention is given to the side-on adsorption complex, it is possible to perceive opposite behavior for Si1 and O2. This is possibly due to the presence of the radical, CH_3 in the first case and the proton in the latter.

The energy scheme for the overall reaction is shown in Figure 5. Because the overall rate of the reaction is slow (due to a very high activation barrier, E_{bar}'') compared to equilibrium

between side-on and end-on, the rate constants for the dehydration can be calculated with respect to the end-on adsorption mode. Table 7 shows the rate constants obtained from TST calculations. The k_r obtained for this reaction is much smaller than that obtained for the hydrogen exchange reaction, due to a much higher activation barrier. Figure 6 shows the Arrhenius plot (ln k_r versus 1000/T) obtained for this reaction. Performing a linear fit of the curves, the Arrhenius activation energy (E_{act}) can be extracted. These values can be seen in the table of Figure 5. E_{act} is always somewhat higher than E_{bar}, as can be observed in the table. In a separated plot of k_{eff}, which is obtained from the product between k_r and K_{eq}, the effective pre-exponents (A_{eff}^{TST}) were obtained. They are shown in Figure 5, and the pre-exponent ratio (A_{eff}^{TST}/A^{HS}) is presented in Table 6. The ratio obtained is somewhat larger for the NLSCF correction ($10^{-3}-10^{-6}$) than for the simple NL correction (10^{-6}). This suggests that the structures obtained in the NLSCF level are looser than those obtained in the NL level. Comparing the ratio obtained in the NLSCF level for both reactions, it is possible to say that the loss in the total entropy is larger for the hydrogen exchange than for the dehydration reaction, due to a higher pre-exponent ratio for the last. But even so, the numbers obtained for this last reaction are quite small and represent considerable loss in the total entropy of the system.

3.3. Normal Mode Frequencies. The harmonic frequencies obtained for the adsorption complexes for both side-on (Figure 1a) and end-on (Figure 4a), at the NLSCF level can be found in Table 11. A comparison with experimental and other theoretical results is shown also in this table. For methanol equilibrium pressure maintained below 10^{-3}, FTIR experiments performed by Mirth et al.[3] reveal three bands which are assigned

TABLE 9: Geometries for the Transition States (TS′, TS″) and Adsorption (Side-On) and Dissociative Complexes for the Reaction of Dehydration (Distances in Angstroms and Angles in Degrees)

	TS′		adsorption complex side-on				TS″				dissociative complex			
	AlH	AlOH	AlH		AlOH		AlH		AlOH		AlH		AlOH	
	NL	NL	NL	NLSCF	NL	NLSCF	NL	NLSCF	NL	NLSCF	NL	NLSCF	NL	NLSCF
O1−H1	0.980	0.980	0.977	0.976	0.979	0.978	0.982	0.983	0.983	0.982	0.978	0.977	0.978	0.977
O1−H2	1.455	1.482	1.480	1.666	1.473	1.631	1.047	1.025	1.043	1.025	0.997	0.990	0.995	0.992
H2−O2	1.055	1.050	1.047	1.018	1.046	1.020	1.606	1.792	1.626	1.769	1.784	1.898	1.786	1.901
O3−C[a]	3.071	3.110	3.061	3.337	3.120	3.380	1.979	2.095	1.988	2.098	1.445	1.478	1.444	1.475
C−O1	1.437	1.434	1.435	1.457	1.433	1.457	1.893	1.919	1.899	1.924	2.906	3.196	2.913	3.244
C−H3	1.103	1.104	1.106	1.100	1.104	1.099	1.093	1.085	1.093	1.085	1.107	1.100	1.103	1.101
C−H4	1.106	1.107	1.107	1.105	1.109	1.105	1.100	1.097	1.101	1.097	1.106	1.103	1.106	1.102
C−H5	1.106	1.106	1.106	1.106	1.107	1.105	1.087	1.082	1.087	1.083	1.103	1.099	1.108	1.099
Si1−O2	1.698	1.719	1.696	1.721	1.715	1.737	1.665	1.677	1.666	1.681	1.652	1.669	1.653	1.668
Al−O2	1.020	1.881	1.938	2.013	1.880	1.941	1.863	1.885	1.821	1.846	1.765	1.787	1.749	1.768
Al−O3	1.763	1.737	1.764	1.782	1.733	1.748	1.869	1.890	1.829	1.855	1.947	2.021	1.896	1.946
Si2−O3	1.639	1.647	1.642	1.657	1.637	1.653	1.669	1.681	1.673	1.687	1.711	1.726	1.721	1.742
Si1−O2−Al	114.50	114.94	121.27	124.13	114.34	115.49	119.80	120.61	117.89	119.51	131.09	126.91	131.39	129.52
O2−Al−O3	99.04	102.89	95.49	94.93	102.85	103.57	106.75	105.81	108.55	108.00	101.83	97.79	102.75	102.33
Si2−O3−Al	130.76	127.67	127.68	129.21	132.06	134.86	118.56	121.57	119.06	121.12	111.44	121.23	112.16	116.35

[a] For the TS′, the distance O3−H5 (in Å): AlH/NL = 2.399; AlOH/NL = 2.391. For the adsorption complex, the distance O3−H3: ALH/NL = 2.188; AlH/NLSCF = 2.667; AlOH/NL = 2.473; AlOH/NLSCF = 2.728.

TABLE 10: Mulliken Charges for the Transition States (TS′, TS″) and Adsorption (Side-On) and Dissociative Complexes for the Reaction of Dehydration

|	TS′		adsorption complex side-on				TS″				dissociative complex			
	AlH	AlOH	AlH		AlOH		AlH		AlOH		AlH		AlOH	
	NL	NL	NL	NLSCF	NL	NLSCF	NL	NLSCF	NL	NLSCF	NL	NLSCF	NL	NLSCF
O1	−0.584	−0.580	−0.606	−0.616	−0.590	−0.607	−0.695	−0.686	−0.693	−0.684	−0.860	−0.848	−0.857	−0.847
H1	0.462	0.464	0.459	0.432	0.461	0.435	0.450	0.440	0.450	0.439	0.416	0.3.99	0.416	0.400
H2	0.525	0.526	0.533	0.540	0.532	0.542	0.467	0.477	0.470	0.478	0.428	0.442	0.426	0.443
C	−0.567	−0.565	−0.564	−0.465	−0.565	−0.478	−0.522	−0.446	−0.524	−0.449	−0.561	−0.460	−0.556	−0.459
H3	0.269	0.267	0.306	0.270	0.296	0.269	0.318	0.312	0.327	0.318	0.289	0.277	0.287	0.288
H4	0.256	0.257	0.232	0.213	0.233	0.219	0.307	0.284	0.308	0.286	0.258	0.228	0.259	0.229
H5	0.264	0.259	0.249	0.220	0.259	0.228	0.301	0.297	0.302	0.295	0.300	0.277	0.295	0.260
Si1	0.237	0.272	0.264	0.397	0.297	0.425	0.272	0.396	0.298	0.423	0.275	0.398	0.282	0.400
O2	−0.702	−0.694	−0.707	−0.767	−0.699	−0.767	−0.727	−0.790	−0.710	−0.782	−0.658	−0.738	−0.643	−0.723
Al	0.271	0.707	0.264	0.415	0.708	0.881	0.232	0.399	0.663	0.844	0.301	0.445	0.695	0.883
O3	−0.612	−0.587	−0.622	−0.681	−0.561	−0.642	−0.616	−0.698	−0.599	−0.685	−0.439	−0.540	−0.419	−0.524
Si2	0.242	0.248	0.269	0.388	0.238	0.382	0.269	0.398	0.293	0.423	0.248	0.402	0.299	0.424
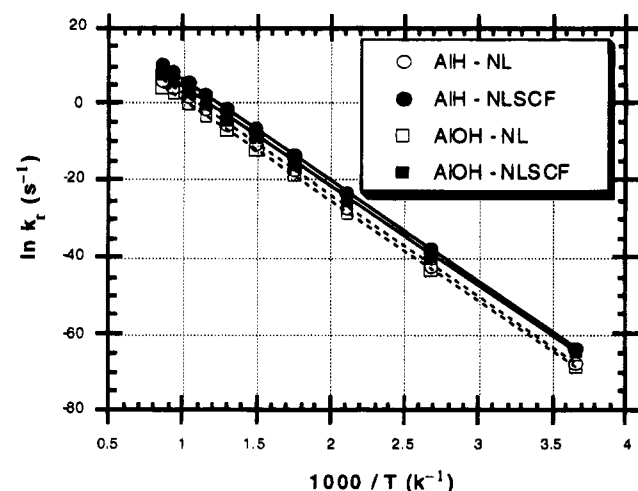
Figure 6. Arrhenius plot: temperature (T) dependence of the natural logarithm of the rate constant, ln k_r, for the reaction of dehydration. The symbols (○, ●, □, ■) represent the calculated ln k_r; the lines (—, - - -), the linear fit.

TABLE 11: Calculated Harmonic Frequencies (cm^{-1}) for Methanol Adsorbed in the Zeolitic Cluster

	side-on		end-on				exptl
	AlOH	AlH	AlOH	AlH	ref 14	ref 15	ref 3
OH stretch							3545[f]
	3676[a]	3692[a]	3237[a]	3245[a]	3276		
	2911[b]	2952[b]				2963[a,e]	2900
			2398[b]	2416[b]	2548	2378[b,e]	2440
CH stretch	3120	3112	3086	3075	3022	3167	2993
	3045	3046	3054	3058	2981	3088	2958
	2970	2979	2972	2973	2889	3046	2856
OH bend							1687[g]
	1364[a,c]	1351[a,c]	1496[a,c]	1483[a,c]	1421[a,c]	1392	
	1255[b,c]	1258[b,c]	1372[b,c]	1349[b,c]	1353[b,c]		
	1116[b,d]	1108[b,d]	1055[b,d]	1040[b,d]	1015[b,d]		

[a] Methanol. [b] Framework. [c] In-Plane. [d] Out-of-plane. [e] Reference 16 has assigned the OH stretch of methanol at 3593 cm^{-1} and that of framework at 3273 cm^{-1}. [f] This band has been assigned as due to OH stretch. At high coverage, together with the bands at 2900, 2440, and 1687 cm^{-1}, this band disappears and new bands at 3280 and 1580 cm^{-1} appear. [g] This band has been assigned by ref 3 as due to OH bend. Actually, together with 2440 and 2993, they form the A-B-C pattern of perturbed framework OH.

to OH stretches (3545, 2900, and 2440), three bands due to CH stretches (2993, 2958, and 2856), and one band corresponding to an OH bending mode (1687), all in cm^{-1}. If the pressure is increased above 10^{-3} mbar to 1 mbar, the bands at 3545, 2900, 2440, and 1687 cm^{-1} disappear and new bands at 3325 cm^{-1} (or 3280 for 1 mbar) and at 1580 cm^{-1} appear. The

calculations presented in this paper refer to the low-pressure results. The experimental features observed at higher pressures are related to solvation effects due to methanol aggregate formation.

Comparing the results obtained in the present work with those obtained by Mirth et al.,[3] one might be tempted to think that

Brønsted-Acid-Activated Methanol

J. Phys. Chem., Vol. 99, No. 30, 1995 **11737**

the OH stretching for methanol obtained for the side-on adsorption complex (3676 cm^{-1}) quantitatively reproduces the band found by Mirth et al. at 3545 cm^{-1} for pressures below 10^{-2} mbar. This is, nevertheless an incorrect conclusion due to the fact that according to the equilibrium constants obtained for this side-on adsorption mode (Tables 7 and 8, and the discussion in section 3.2) very few methanol molecules actually adsorb side-on in the zeolite, compared to the end-on mode. This band (at around $3400-3550$ cm^{-1}) has been interpreted by Pelmenschikov et al.[35] as due to formation of $-SiOCH_3$ and $-SiOH$ groups produced by dissociative chemisorption of methanol in the strained siloxane (Si-O-Si) bridges.

The methanol OH stretch for the end-on AlOH/NLSCF complex (3237 cm^{-1}) seems to agree with the findings of Mirth et al.[3a] for the low-pressure spectrum, where a small shoulder at around 3300 cm^{-1} can be observed. This identification cannot be considered, however, as definitive since in ref 3b the infrared spectrum of methanol adsorbed into a different sample of HZSM5 does not reproduce this shoulder. In the same paper, however, for methanol adsorbed into HNaY, small adsorption features are also presented between 3200 and 3400 cm^{-1}. Theoretical work of Haase and Sauer[14] reported also a band at 3276 cm^{-1}, near to that obtained in the present study. Gale et al.[15] assigned a band at 2963 cm^{-1} as being due to OH stretching of the methanol and at 2378 cm^{-1} as due to framework for the end-on structure. The band at 2963 cm^{-1} is to be compared to 3237 cm^{-1} obtained in this work. It has been shown previously that the $O_{methanol}-H_{methanol}$ distance obtained in the present study and the one of Gale et al.,[15] both at the DFT/AlOH/NLSCF level, are exactly the same, 1.005 Å. On the other hand, the $O_{framework}-H_{framework}$ bond distance calculated by Gale et al. is longer, and as a consequence, the $O_{methanol}-H_{framework}$ distance is shorter than in the present work. As a result, one can conclude that the methanol molecule in Gale's work is more perturbed by the zeolitic proton. This could be the explanation for a lower OH stretch mode found by Gale et al.[15] than in the present work. Bates and Dwyer,[16] performing HF calculations, found frequencies for the OH stretching of methanol and framework that are significantly higher compared to the DFT results. The frequencies obtained at the NL level are not presented since at this level of calculation the zeolitic proton is not correctly described, as discussed in section 3.1.

The other three bands associated by Mirth et al.[3] as being due to OH stretching (2900 and 2440 cm^{-1}) and bending modes (1687 cm^{-1}) are pseudobands due to resonant interactions between the OH stretching of the zeolite and an overtone bending mode of the perturbed bridging OH groups, the A-B-C bands.[36] This OH−complex band consists of three subbands, which appear at ≈ 2800, ≈ 2400, and ≈ 1700 cm^{-1}. Calculations of the harmonic frequencies result in the appearance of only one of those three bands, expected to be around 2500 cm^{-1}. For the end-on complex, the only band calculated is nearly 2400 cm^{-1}, somewhat lower than expected. The bands for the OH in-plane bending mode of methanol and framework were found to be nearly 1490 and 1360 cm^{-1}, and for out-of-plane, at 1050 cm^{-1}. Haase and Sauer[14] find them at 1421, 1353, and 1015 cm^{-1}, respectively. The computed CH stretching modes for the end-on adsorption mode (3080, 3055, and 2970 cm^{-1}) are higher than the ones obtained experimentally (2993, 2958, and 2856 cm^{-1}) and lower than the ones obtained by another DFT calculation[15] (3167, 3088, and 3046 cm^{-1}).

4. Conclusions

The reactions of hydrogen exchange and dehydration of methanol catalyzed by an acidic zeolite have been studied using the DFT method. Equilibrium constants for the adsorption modes have been evaluated, and reaction rate constants have been calculated by means of transition state reaction rate theory.

For the hydrogen exchange reaction, it has been found that methanol is hydrogen-bonded to the zeolite cluster model in a way that the hydroxyl group is directed to the zeolite cluster model (end-on). The previously proposed chemisorbed methoxonium ion was found to be, in reality, a transition state rather than a chemisorbed species, in agreement with other theoretical work.[13-15] The activation barrier found in this study is rather low, 11 kJ/mol for the AlOH/NLSCF level. The rate-limiting step for the overall reaction is then not the activation barrier but the desorption process, nearly -70 kJ/mol.

Methanol can also adsorb in the zeolite in a way where the carbon atom is directed to the basic lattice oxygen and the oxygen of the hydroxyl group is directed to the zeolitic proton, namely, side-on. The calculated equilibrium constants between reactants and this side-on adsorption mode are very low compared to end-on, and only at very high temperatures will this mode of adsorption be populated. The dehydration reaction of methanol by an acidic zeolite is believed then to initiate via the end-on adsorption mode. The methanol molecule goes through the side-on adsorption mode by a fast equilibration reaction. The activation barrier for the overall dehydration reaction with respect to the end-on adsorption mode in the AlOH/NLSCF level is $+66$ kJ/mol, nearly 14 kJ/mol lower than the experimental value.[6] In the transition state, the CH_3 group resembles the carbenium ion, very similar to the result for the dehydrogenation of methane.[24,34] Its total Mulliken charge is $+0.4$, and hybridization of the carbon atom is close to sp^2. This group is electrostatically stabilized by the zeolitic cluster. In the final state a strongly bonded methoxy group is formed as well as physically adsorbed H_2O.

An analysis of the harmonic frequencies of the end-on adsorption complex seems to confirm the end-on adsorption mode of adsorbed methanol. It is essential to consider the Fermi resonance of the downward-shifted OH frequencies to assign the experimental bands. The two bands at 2900 and 2440 cm^{-1} (due to OH stretches) combined with a band at 1687 cm^{-1} (due to OH bending mode) are pseudobands due to the resonant interaction between the OH stretching of the zeolite and the overtone bending mode of the perturbed bridging OH groups, the A-B-C bands.[36] In the calculation of harmonic frequencies, only one of those three A-B-C bands is actually observed. For the end-on adsorption complex it is approximately at 2400 cm^{-1}.

The elementary reaction rate constants for the hydrogen exchange reaction are large due to a very low activation barrier. The ratio A_{eff}^{TST}/A^{TS}, is very small, especially when the NLSCF correction is used, showing a large loss in entropy of the system compared to gas phase methanol molecule. For the dehydration reaction, the rate constants are rather small compared to hydrogen exchange, due to a higher activation barrier. The loss in the transition state entropy is less than for the hydrogen exchange reaction.

The geometry of the adsorption complex for the hydrogen exchange reaction is strongly dependent on NLSCF correction. If the correction is added only at the end of the geometry optimization, the NL correction, the distances $O_{methanol}-H_{framework}$ and $H_{framework}-O_{framework}$ are too short and too long, respectively. This is reflected in the frequencies that are then a mixture between the adsorption complex and the transition state.

References and Notes

(1) (a) Meisel, S. L.; McCullogh, J. P.; Lechthaler, C. H.; Weisz, P. B. *CHEMTECH* **1976**, *6*, 86. (b) Chang, C. D. *Hydrocarbons from Methanol*; Marcel Dekker: New York, 1983.

(2) (a) Tsiao, C.; Corbin, D. R.; Dybowski, C. *J. Am. Chem. Soc.* **1990**, *112*, 7140. (b) Anderson, M. W.; Klinowski, J. *J. Am. Chem. Soc.* **1990**, *112*, 10. (c) Murray, D. K.; Chang, J.-W.; Haw, J. F. *J. Am. Chem. Soc.* **1993**, *115*, 4732.

(3) (a) Mirth, G.; Lercher, J. A.; Anderson, M. W.; Klinowski, J. *J. Chem. Soc., Faraday Trans.* **1990**, *86*, 3039. (b) Mirth, G.; Kogelbauer, A.; Lercher, J. A. *In Proceedings of the 7th International Zeolite Conference*, Montreal 1992; von Ballamos, R., Higgins, J. B., Treacy, M. M. J., Eds.; Butterworths: London, 1993; p 251.

(4) (a) Klinowski, J.; Anderson, M. W. *J. Magn. Reson.* **1990**, *28*, S68. (b) Klinowski, J. *Chem. Rev.* **1991**, *91*, 1459. (c) Pope, C. G. *J. Chem. Soc., Faraday Trans.* **1993**, *89*, 1139.

(5) Bosácek, V. *J. Phys. Chem.* **1993**, *97*, 10732.

(6) Bandiera, J.; Naccache, C. *Appl. Catal.* **1991**, *69*, 139.

(7) Messow, U.; Quitzsch, K.; Herden, H. *Zeolites* **1984**, *4*, 255.

(8) Hocevar, S.; Levec, J. *J. Catal.* **1992**, *135*, 518.

(9) (a) Jackson, J. E.; Bertsch, F. M. *J. Am. Chem. Soc.* **1990**, *112*, 9085. (b) Luk'yanov, D. B. *Zeolites* **1992**, *12*, 287. (c) Sulikowski, B.; Klinowski, J. *Appl. Catal. A: General* **1992**, *89*, 69. (d) Hutchings, G. J; Lee, D. F.; Lynch, M. *Appl. Catal. A: General* **1993**, *106*, 115.

(10) Vetrivel, R.; Catlow, C. R. A.; Colbourn, E. A. *J. Phys. Chem.* **1989**, *93*, 4594.

(11) Gale, J. D.; Catlow, C. R. A.; Cheetham, A. K. *J. Chem. Soc., Chem. Commun.* **1991**, *3*, 178.

(12) Sauer, J.; Kölmel, C.; Haase, F.; Ahlrichs, R. *In Proceedings of the 7th International Zeolite Conference*, Montreal 1992; von Ballamos, R., Higgins, J. B., Treacy, M. M. J., Eds.; Butterworths: London, 1993; p 679.

(13) Haase, F.; Sauer, J. *J. Phys. Chem.* **1994**, *98*, 3083.

(14) (a) Haase, F.; Sauer, J. Submitted for publication in *J. Am. Chem. Soc.* (b) Sauer, U.; Ugliengo, P.; Garrone, E.; Saunders, V. R. *Chem. Rev.* **1994**, *94*, 2095.

(15) Gale, J. D.; Catlow, C. R. A.; Carruthers, J. R. *Chem. Phys. Lett.* **1993**, *216*, 155.

(16) Bates, S.; Dwyer, J. *J. Mol. Struct. (THEOCHEM)* **1994**, *306*, 57.

(17) Senchenya, I. N.; Frash, M. V.; Kazansky, V. B.; van Santen, R. A. Manuscript in preparation.

(18) (a) Hohenberg, P.; Kohn, W. *Phys. Rev. B* **1964**, *136*, 864. (b) Kohn, W.; Sham, L. J. *Phys. Rev. A* **1965**, *140*, 1133.

(19) Andzelm, J.; Wimmer, E. *J. Chem. Phys.* **1992**, *96*, 1280.

(20) Vosko, S. H.; Wilk, L.; Nusair, M. *Can. J. Phys.* **1980**, *58*, 1200.

(21) Perdew, J .P. *Phys. Rev. B* **1986**, *33*, 8822.

(22) Becke, A. D. *Phys. Rev. A* **1988**, *38*, 3098.

(23) Fan, L.; Ziegler, T. *J. Am. Chem. Soc.* **1992**, *114*, 10890.

(24) Blaszkowski, S. R.; Jansen, A. P. J.; Nascimento, M. A. C.; van Santen, R. A. *J. Phys. Chem.* **1994**, *98*, 12938.

(25) Godbout, N.; Andzelm, J.; Wimmer, E.; Salahub, D. R. *Can. J. Chem.* **1992**, *70*, 560.

(26) (a) Sauer, J. *Chem. Rev.* **1989**, *89*, 199. (b) Radzio, E.; Andzelm, J.; Salahub, D. R. *J. Comput. Chem.* **1985**, *6*, 553.

(27) Andzelm, J.; Russo, N.; Salahub, D. R. *Chem. Phys. Lett.* **1987**, *142*, 169.

(28) (a) Shlegel, H. B. *Ab Initio Methods in Quantun Chemistry*; Lawley, K. P., Ed.; John Wiley & Sons: New York; 1987. (b) Head, J. D.; Zerner, M. C. *Adv. Quantum Chem.* **1989**, *20*, 239.

(29) McIver, J. W.; Komornicki, A. *Chem. Phys. Lett.* **1971**, *10*, 303.

(30) Wilson, E. B.; Decius, J. C.; Cross, P. C. *Molecular Vibrations*; Mc Graw-Hill: New York; 1955.

(31) (a) Frost, A. A.; Pearson, R. G. *Kinetics and Mechanisms*; John Wiley & Sons: New York, 1961. (b) Moore, J. W.; Pearson, R. G. *Kinetics and Mechanisms*; John Wiley & Sons: New York, 1981. (c) Gilbert, R. G.; Smith, S. C. *Theory of Unimolecular and Recombination Reactions*; Blackwell Scientific Publications: Oxford, 1990.

(32) Ziegler, T. *Chem. Rev.* **1991**, *91*, 651.

(33) (a) Brand, H. V.; Curtiss, L. A.; Iton, L. E. *J. Phys. Chem.* **1992**, *96*, 7725. (b) Brand, H. V.; Curtiss, L. A.; Iton, L. E. *J. Phys. Chem.* **1993**, *97*, 12773.

(34) Kazansky, V. B.; Frash, M. V.; van Santen, R. A. *Catal. Lett.* **1994**, *28*, 211.

(35) (a) Pelmenschikov, A. G.; Morosi, G.; Gamba, A. *J. Phys. Chem.* **1992**, *96*, 2241. (b) Pelmenschikov, A. G.; Morosi, G.; Gamba, A.; Zecchina, A.; Bordiga, S.; Paukshtis, E. A. *J. Phys. Chem.* **1993**, *97*, 11979.

(36) Pelmenschikov, A. G.; van Santen, R. A.; Jänchen, J.; Meijer, E. *J. Phys. Chem.* **1993**, *97*, 11071.